INSTITUTO DE FÍSICA

preprint

IFUSP/P-248

APPLICATIONS OF PARTIAL DIFFERENTIAL APPROXIMANTS: TEST FUNCTIONS AND DIMENSIONAL CROSSOVER IN THE ISING MODEL

by

J.F. Stilck and S.R. Salinas

Instituto de Física, Universidade de São Paulo
C.P. 20516, São Paulo, SP, Brazil

UNIVERSIDADE DE SÃO PAULO
INSTITUTO DE FÍSICA
Caixa Postal - 20.516
Cidade Universitária
São Paulo - BRASIL

"APPLICATIONS OF PARTIAL DIFFERENTIAL APPROXIMANTS: TEST FUNCTIONS AND DIMENSIONAL CROSSOVER IN THE ISING MODEL"

J.F. Stilck and S.R. Salinas

Instituto de Física, Universidade de São Paulo

C.P. 20516, São Paulo, SP, Brazil

ABSTRACT

The method of partial differential approximants (PDA) has been introduced for approximating functions of two or more variables given a finite number of coefficients of their power series. It is supposed to be effective close to the multicritical points, where the thermodynamic functions are expected to behave according to the scaling hypothesis. In order to assess the performance of the method, we have undertaken the construction of PDA's for several test functions of two variables. For some simple functions, which are represented exactly by PDA's and which exhibit an analog of a multicritical point, the numerical estimates yielded very good results even at lower orders. For other functions the estimates tended to improve as we increased the order of the approximants. For the best PDA's we constructed flow diagrams and estimated the scaling functions. Also, we have analyzed the dimensional crossover (from $d = 3$ to $d = 2$) of the spin - 1/2 axial anisotropic Ising model on the f cc lattice. We considered series expansions for the direct susceptibility and also for the sum of the direct and the staggered susceptibilities. In general, our estimates agree with the scaling predictions.

I. INTRODUCTION

The usefulness of the Padé method for approximating functions of one variable given a finite number of coefficients of their power series is appreciated widely. In the theory of critical phenomena, for instance, the so-called d-log Padé approximants have been very practical for providing estimates of the critical parameters of thermodynamic model functions (Hunter and Baker 1973, Baker and Hunter 1973). These successes have stimulated some recent proposals to generalize the Padé method for approximating functions of two or more variables (Chisholm 1973, Roberts et al. 1975). The present publication refers to a proposal by Fisher (1977a, 1977b), which seems particularly suited for analyzing the scaling behavior of thermodynamic model functions in the neighborhood of their multicritical points.

In the conventional d-log Padé method (Baker 1975) the logarithmic derivative of a function $f(x)$ is approximated as

$$\frac{d}{dx} \ell n\, f(x) \approx \frac{P_L(x)}{Q_M(x)} = \frac{d}{dx} \ell n\, F_{LM}(x) \qquad (1.1)$$

where $P_L(x)$ and $Q_M(x)$ are polynomials of degrees L and M respectively. These rational approximants may represent well branch point singularities of the form

$$f(x) \approx A(x_c - x)^{-\gamma} \quad \text{for} \quad x \to x_c^- \,, \qquad (1.2)$$

where γ is a nonintegral exponent. One should recall at this point that the approximants $F_{LM}(x)$ may also be regarded as the solutions of the differential equation

$$P_L(x)\, F_{LM}(x) = Q_M(x)\, \frac{d}{dx} F_{LM}(x) \quad . \tag{1.3}$$

The coefficients p_ℓ and q_m ($\ell = 0,1,\ldots,L$; $m = 0,1,\ldots,M$) of the polynomials P_L and Q_M in powers of x are then chosen so that the power series solution of Eq. (1.3) agrees with the expansion of $f(x)$ to optimal order. In the critical region we have

$$Q_M(x) \simeq Q_c'(x - x_c) \tag{1.4a}$$

and

$$P(x_c) = P_c = -\gamma\, Q_c' \quad , \tag{1.4b}$$

which provide estimates of x_c and γ.

Let us consider a function of two variables x and y, given by the series expansion

$$f(x,y) = \sum_{k,k'=0} f_{k,k'}\, x^k\, y^{k'} \quad , \tag{1.5}$$

where the indices k and k' belong to some set of integers $\underset{\sim}{K}$. In analogy with Eq. (1.3), Fisher (1977a, 1977b) proposed a novel class of approximants for these functions, $F_{LMN}(x,y)$, defined as the solutions of the partial differential equation

$$P_L(x,y)F(x,y) = Q_M(x,y)\,\frac{\partial F(x,y)}{\partial x} + R_N(x,y)\,\frac{\partial F(x,y)}{\partial y} \qquad (1.6)$$

subjected to suitable boundary conditions. The polynomials P_L, Q_M and R_N are chosen so that the series solution for $F(x,y)$ in powers of x and y agrees with the known expansion (1.5) as far as possible. This simply leads to a set of simultaneous linear equations which may be solved by standard numerical methods.

As we stated above, these "partial differential approximants" (which will be called PDA) are particularly effective when $f(x,y)$ displays a singular behavior according to the scaling hypothesis of the theory of critical phenomena, that is, for

$$f(x,y) \approx |\Delta x|^{-\gamma}\, Z\left(\frac{\Delta y}{|\Delta x|^{\phi}}\right) , \qquad (1.7)$$

as $\Delta x \equiv x_c - x \to 0$ and $\Delta y \equiv y_c - y \to 0$, where γ and ϕ are two exponents, in general nonintegral, while $Z(z)$ is a "scaling function" of a single variable z. In this case, it is easy to see that the multicritical point will be estimated by

$$Q_M(x_c,y_c) = R_N(x_c,y_c) = 0 \qquad (1.8)$$

while the rate of variation of R_N and Q_M at the multicritical point, normalized by $P_c = P_L(x_c,y_c)$, will give estimates for the exponents γ and ϕ.

To these days, except for some exploratory

trials, partial differential approximants have been tested only in the problem of the anisotropic exchange crossover in three-dimensional classical ferromagnets (Fisher and Kerr 1977). As far as we know, there have been no applications either to other physical problems of interest or to some model examples. The main point of our paper is thus to contribute for assessing the potentialities of the method by investigating numerically some classes of test functions, and also the dimensional crossover in the Ising model. We believe that our tests will reveal the advantages and some drawbacks (slow convergence, the need for longer series) of these partial differential approximants.

The layout of our paper is as follows. In Sec. II we consider a more general scaling form, where the scaling axes are not parallel to the cartesian axes, and introduce the method of characteristics for obtaining the numerical solutions of the partial differential equation (1.6). Also, we discuss the criteria for the stability of these solutions near the multicritical points. In Sec. III we study several model functions, some of which can be represented exactly by PDA's. We obtain the multicritical parameters, some flow diagrams, and try to compare the performance of different orders of PDA's. Sec. IV is about the analysis of the dimensional crossover, between dimensions $d = 3$ and $d=2$, of the Ising model with lattice anisotropy. In particular, we use the PDA's for estimating the shape of the phase boundaries in the temperature-anisotropy phase diagram. Finally, a summary is presented in Sec. V.

II. FURTHER DESCRIPTION OF THE METHOD

In general, the scaling axes are not parallel to the cartesian x,y axes. We thus have the scaling form

$$f(x,y) \approx |\Delta\tilde{x}|^{-\gamma} \; Z\left(\frac{\Delta\tilde{y}}{|\Delta\tilde{x}|^{\phi}}\right) , \tag{2.1}$$

where

$$\Delta\tilde{x} = \Delta x - \frac{1}{e_2}\,\Delta y , \tag{2.2}$$

and

$$\Delta\tilde{y} = \Delta y - e_1\,\Delta x . \tag{2.3}$$

The parameters e_1 and e_2 represent the slopes of the optimal scaling axes in the cartesian coordinate system specified by x and y.

The scaling form of Eq. (2.1) obeys the partial differential equation

$$(\Delta\tilde{x} + \frac{\phi}{e_2}\,\Delta\tilde{y})\,\frac{\partial f}{\partial x} + (e_1\,\Delta\tilde{x} + \phi\,\Delta\tilde{y})\,\frac{\partial f}{\partial y} =$$

$$= -\gamma(1 - \frac{e_1}{e_2})\,f , \tag{2.4}$$

which should be compared, in the vicinity of the multicritical point (x_c,y_c), with the defining differential equation (1.6)

of the PDA's. If the polynomials P_L , Q_M and R_N in leading order close to the multicritical point are given by

$$P_L(x,y) \simeq P_c \quad , \tag{2.5}$$

$$Q_M(x,y) \simeq Q_1 \Delta x + Q_2 \Delta y \quad , \tag{2.6}$$

$$R_N(x,y) \simeq R_1 \Delta x + R_2 \Delta y \quad , \tag{2.7}$$

we may write the following expressions for the slopes of the scaling axes and the multicritical exponents,

$$e_{1,2} = \frac{1}{2} \frac{R_2 - R_1}{Q_2} \pm \frac{1}{2} \left[\left(\frac{R_2 - R_1}{Q_2} \right)^2 + 4 \frac{R_1}{Q_2} \right]^{1/2} \quad , \tag{2.8}$$

$$\gamma = \frac{P_c}{e_2 Q_2 - R_2} \quad , \tag{2.9}$$

and

$$\phi = -1 - \gamma \frac{Q_1 + R_2}{P_c} \quad . \tag{2.10}$$

Thus the estimate for the location of the multicritical point is given by $Q_M(x_c,y_c) = R_N(x_c,y_c) = 0$, while e_1 , e_2 , γ and ϕ , are related to the rate of change of the polynomials Q_M and R_N at the estimated values (x_c,y_c) provided that $P_L(x_c,y_c) \neq 0$.

To estimate the actual values assumed by f(x,y),

Fisher (1977a) suggested the numerical solution of Eq. (1.6) via the method of characteristics. In the multicritical region, this corresponds to the evaluation of the scaling function $Z(z)$, which is often of interest in the theory of critical phenomena. Let us consider a time-like variable t such that

$$x = x(t) \quad , \quad y = y(t) \quad , \tag{2.11}$$

and

$$\frac{dx}{dt} = Q_M(x,y) \quad , \quad \frac{dy}{dt} = R_N(x,y) \quad . \tag{2.12}$$

From Eq. (1.6) we have

$$P_L(x,y)\ f(x,y) = \frac{d}{dt}\ f(x,y) \quad , \tag{2.13}$$

and, therefore,

$$f\Big[x(t),y(t)\Big] - f\Big[x(0),y(0)\Big] = \exp\left\{\int_0^t P_L\Big[x(t'),y(t')\Big]\ dt'\right\} \ , \tag{2.14}$$

where it should be stressed that the integration is performed along the trajectories defined by Eq. (2.12). Given the polynomials $Q_M(x,y)$ and $R_N(x,y)$, the problem is then reduced to the solution of the set of coupled ordinary differential equations (2.12).

In problems of physical interest it is often important to know the loci of the singularities of the functions

$f(x,y)$ (for instance, the shapes of the phase boundaries near the bicritical point of an antiferromagnet in the field-temperature phase diagram). From Eq. (2.14), since $P_L(x,y)$ is a finite polynomial, there is a finite difference between the values assumed by the function $f(x,y)$, calculated at two points which lie on the same trajectory. Therefore, the critical lines, where $f(x,y)$ is supposed to diverge, are flow-lines defined by Eqs. (2.12). It is enough to know one single point on these trajectories, besides the multicritical point, to be able to construct them numerically. An illuminating application of this procedure, which will become more transparent in the following sections, is presented in the paper of Fisher and Kerr (1977).

In the neighborhood of the estimated multicritical point (x_c,y_c), Eqs. (2.12) may be written as the linearized forms

$$\frac{dx}{dt} = Q_1 \Delta x + Q_2 \Delta y \quad , \tag{2.15a}$$

and

$$\frac{dy}{dt} = R_1 \Delta x + R_2 \Delta y \quad , \tag{2.15b}$$

which have the general solution

$$\Delta x = C_1 \exp(\lambda_1 t) + C_2 \exp(\lambda_2 t) \quad , \tag{2.16a}$$

and

$$\Delta y = C_1 e_1 \exp(\lambda_1 t) + C_2 e_2 \exp(\lambda_2 t) \quad , \qquad (2.16b)$$

where C_1 and C_2 are arbitrary constants. The particular solutions with $C_1 = 0$ or $C_2 = 0$ define the scaling axes, and the eigenvalues λ_1 and λ_2 are given by

$$\lambda_{1,2} = \frac{1}{2}(Q_1 + R_2) \pm \frac{1}{2}\left[(Q_1 - R_2)^2 + 4Q_2R_1\right] = Q_2 e_{1,2} + Q_1 \qquad (2.17)$$

A complete discussion about the stability of Eqs. (2.16), which will define the behavior of the flow-lines in the immediate vicinity of the estimated multicritical point, may be found, for example, in the book by Brand (1966). In the case where λ_1 , $\lambda_2 < 0$, all flow-lines in the neighborhood of (x_c, y_c) converge onto this estimated multicritical point. Although it is desirable to have a stable multicritical point, this is not strictly necessary for performing numerical evaluations of the function $f(x,y)$. The estimated values of (x_c, y_c) may happen to be a saddle point (for $\lambda_1 \lambda_2 < 0$) or even a star-like unstable node.

Another interesting feature of the flow diagrams is the following expression for the slope of the flow lines in the immediate vicinity of the estimated multicritical point,

$$\frac{dy}{dx} = \frac{C_1 \lambda_1 e_1 \exp(\lambda_1 t) + C_2 \lambda_2 e_2 \exp(\lambda_2 t)}{C_1 \lambda_1 \exp(\lambda_1 t) + C_2 \lambda_2 \exp(\lambda_2 t)} \quad . \qquad (2.18)$$

For $\lambda_1 < \lambda_2 < 0$, unless $C_2 = 0$, the value of dy/dx tends to

the slope e_2 of the scaling axis as $t \to \infty$. This will become apparent in the analysis of the model functions which are considered in the next section.

Finally, a relevant question concerns the magnitude of the region where the predictions of the linear approximation still work. This may be estimated by the standard techniques associated with the Liapunov functions (Brand 1966).

III. NUMERICAL RESULTS WITH TEST FUNCTIONS

We applied the technique of partial differential approximants to obtain numerical estimates pertaining to the following model functions:

(i) functions with one line of singularities

$$F_a = (1 - 2x - y)^{-3/2} \tag{3.1}$$

$$F_b = (1 - 2x - y)^{-3/2} \exp(-y) \tag{3.2}$$

(ii) functions with two lines of singularities

$$F_c = (1 - x - \tfrac{1}{2} y)^{-3/2} (1 - 2x - \tfrac{1}{5} y)^{-1/2} \tag{3.3}$$

$$F_d = (1-x-2y)^{-5/2} (1-3x-y)^{-2} \ln(1-3x-y) \tag{3.4}$$

$$F_e = (1-x-\frac{1}{2}y)^{-3/2}(1-2x-\frac{1}{5}y)^{-1/2} + \exp(-x-2y)\cos(xy) \quad (3.5)$$

$$F_f = (1-x-2y)^{-5/2}\,(1-3x-y)^{-2} + \exp(-x-2y)\cos(xy) \quad (3.6)$$

Functions F_a to F_d are represented exactly by PDA's of lower orders (as remarked by Fisher (1977a), they belong to a general class of functions which may be represented exactly). Roberts et al. (1975) have analyzed similar functions by the techniques of Canterbury approximants. Also, these functions may be regarded as the natural extensions of the one-variables functions which had been analized by the Padé method and other techniques by Hunter and Baker (1973).

The singular parts of the test functions (3.3) to (3.6) obey the general scaling form of Eq. (2.1) with two options for the scaling function $Z(z)$. For example, in the case of functions F_c and F_e, one of the options is

$$\Delta\tilde{x} = 1 - x - \frac{1}{2}y \quad , \qquad (3.7a)$$

and

$$\Delta\tilde{y} = 1 - 2x - \frac{1}{5}y \quad , \qquad (3.7b)$$

which leads to

$$e_1 = -10 \ , \ e_2 = -2 \ , \ \gamma - \frac{1}{2}\phi = \frac{3}{2} \ , \text{ and } \ Z(z) = z^{-1/2} \ .$$

In the other option $\Delta\tilde{x}$ and $\Delta\tilde{y}$ are interchanged, leading to

$$e_1 = -2 \ , \ e_2 = -10 \ , \ \gamma - \frac{3}{2}\phi = \frac{1}{2} \ , \text{ and } \ Z(z) = z^{-3/2} \ .$$

For these functions, unlike in the case of the real physical problems, it is not possible to determine γ and ϕ independently. Also, it should be remarked that F_c may be represented exactly by a set of PDA's where P_L has a constant value and the polynomials Q_M and R_N are linear in the variables x and y.

Functions F_a to F_f were represented as the power series

$$F(x,y) = \sum_{k,k'=0} f_{k,k'} \, x^k y^{k'} \tag{3.8}$$

with the coefficients $f_{k,k'}$ corresponding to a triangular array (that is, with $k + k' \leq o_S$, where the integer o_S gives the order of the series). Also, the polynomials P_L, Q_M, and R_N are given by the triangular arrays,

$$P_L(x,y) = \sum_{\ell,\ell'=0} p_{\ell,\ell'} \, x^{\ell} y^{\ell'} \ , \tag{3.9}$$

$$Q_M(x,y) = \sum_{m,m'=0} q_{m,m'} \, x^m y^{m'} \ , \tag{3.10}$$

and

$$R_N(x,y) = \sum_{n,n'=0} r_{n,n'} x^n y^{n'} \quad , \tag{3.11}$$

where the integers L, M and N, are the number of terms of the polynomials P_L, Q_M and R_N, respectively, and $\ell + \ell' \leq o_P$, $m + m' \leq o_Q$, and $n + n' \leq o_R$. As we are fixing L, M and N, instead of the order o_P, o_Q, and o_R, the polynomials P_L, Q_M and R_N may not be symmetric in terms of the variables x and y. For example, the polynomial P_L, with $L = 4$, is written as

$$P_4(x,y) = p_{00} + p_{10}x + p_{01}y + p_{20}x^2 \quad . \tag{3.12}$$

If we make $p_{00} = 1$, the $L+M+N-1$ remaining coefficients of the polynomials are determined by the set of linear equations which come from the substitution of the series expansion (3.8) into Eq. (1.6). Given a series of order o_S, we may construct approximants of order o_A, such that

$$o_A \leq o_S - 1 \quad , \tag{3.13}$$

where

$$L + M + N - 1 = \frac{(o_A+1)(o_A+2)}{2} \equiv K(o_A) \quad . \tag{3.14}$$

The construction of all PDA's up to a certain order, in analogy with the standard Padé tables, is a rather formidable task even at not so high orders. Indeed, the number of approximants

of order o_A is given by

$$K\left[K(o_A)\right] = \frac{(o_A+1)^2(o_A+2)^2}{8} + \frac{3}{4}(o_A+1)(o_A+2) + 1 \quad . \qquad (3.15)$$

This clearly imposes sharp limitations on the numerical calculations. Therefore, we have chosen 88 approximants, up to order 13, in a somewhat arbitrary fashion. As defined in Table I, we included diagonal and near-diagonal approximants ($L \approx M \approx N$), as well as some off-diagonal ones.

It has been impossible to construct numerical approximants for F_a, even at the lowest orders, due to ill conditioned equations. With the exception of some off-diagonal approximants, the estimates for the critical points of F_b lie along the critical line, and tend to cluster around the intersection with the cartesian axes. For F_c and F_d, even at the lowest orders, we obtained nearly exact results for the multicritical points, the slopes of the scaling axes and the multicritical exponents. However, some off-diagonal approximants give estimates of the multicritical point which concentrate along one of the critical lines. For these functions the system of linear equations tends to become ill conditioned as we increase the order of the PDA's.

Due to the regular terms added to their singular parts, functions F_e and F_f are not represented exactly by finite partial differential approximants. For function F_f the singularities are stronger and closer to the origin than for F_e. So, it was not surprising to verify that F_f is

better represented than F_e with PDA's of lower orders. A sample of the estimates for the multicritical parameters of F_e and F_f is given in Tables II and III respectively. As a general pattern, the quality of the estimates improves as we increase the order of the approximants. Also, diagonal and near-diagonal approximants tend to produce better estimates than off-diagonal ones. Tables IV and V give ordered sequences of approximants according to the decreasing precision of their estimates. By the inspection of these sequences, it becomes apparent that there exists a correlation between the quality of different estimates: usually, a PDA which gives a good estimate of the location of the multicritical point, also happens to produce good estimates of the slopes of the scaling axes and of the multicritical exponents.

After obtaining the estimates of the multicritical parameters, we used the method of characteristics for solving numerically the differential equation (1.6). It turns out that most approximants for F_c to F_f, despite yielding good estimates for the multicritical parameters, display a saddle point unstable multicritical point in their flow-diagrams. As a matter of fact, no correlations were apparent between the quality of the estimates and the stability of the multicritical point.

In Fig. 1 we show the flow-diagram corresponding to the approximant number 1 for F_c ($L=1$, $M=N=3$). Within the numerical precision, this particular approximant belongs to the set of PDA's which represent F_c exactly. Since the polynomials Q_M and R_N are linear in x and y, the

system of coupled ordinary differential equations (2.14) is already linearized, and we can find solutions that hold in all regions of the x,y plane. In particular, since the estimated multicritical point is stable, every flow-line, no matter its starting point, converges onto (x_c, y_c). The characterization of the critical lines as flow-lines, and the asymptotic alignment of the flow-lines with the scaling axis of slope $e_1 = -10$ (associated with the smallest value of $|\lambda|$), are also apparent from Fig. 1. Estimates of F_c along some flow-lines were obtained by the numerical evaluation of Eq. (2.14). Of course, in the case of this particular PDA, the defining equation (1.6) can be solved exactly, so that our numerical calculations could be controlled against the corresponding exact results. For example, in Fig. 1, if we start at the beginning of the flow-lines with the exact value of F_c, after a time interval of about 3 units, which already leads to the vicinity of the multicritical point, the usual error of our computer program amounts to about 0.3%.

The flow-lines corresponding to the approximant number 73 for F_f $(L = 35\ ,\ M = 34\ ,\ N = 37)$ are shown in Fig. 2. This PDA exhibits a stable multicritical point with the same features of the previous one. The asymptotic alignment of the flow-lines with the scaling axis corresponding to $e_1 = -3$ is more striking in this case. This is due to the larger value of the difference $|\lambda_1 - \lambda_2|$. The estimates for F_f have a typical error of about 1% after an interval or 3 time units. In these numerical calculations, we used a Runge-Kutta method of fourth order for obtaining the flow diagrams,

and a Simpson procedure for performing the integrations, without worrying about the precision of the results.

IV. DIMENSIONAL CROSSOVER IN THE ISING MODEL

An Ising model with axial anisotropy may be defined by the Hamiltonian

$$\mathcal{H} = -J \sum_{(i,j)}^{(x,y)} s_i s_j - RJ \sum_{(i,j)}^{(z)} s_i s_j - H \sum_i s_i - H_{st} \sum_i (-1)^{\eta_i} s_i \quad (4.1)$$

where $s_i = \pm 1$, the first sum is over nearest neighbor pairs in the x-y planes, and the second sum is over nearest neighbor pairs whose relative displacement vector has a z component. H stands for the applied magnetic field, and H_{st} for a staggered magnetic field which acts oppositely on adjacent planes of constant z (the parameter η_i is 0 or 1 depending on whether s_i belongs to an even or to an odd x-y plane). In this work we consider $J > 0$ only, so that for $R > 0$ the system orders ferromagnetically, while it exhibits metamagnetic behavior for $R < 0$. The special value $R = 0$ corresponds to a set of uncoupled two-dimensional ferromagnetic Ising models. Therefore, according to the ideas of smoothness and universality, an abrupt change in the values of the critical exponents is expected to occur at $R = 0$. The method of partial differential approximants is quite suitable for studying this dimensional crossover between $d = 3$ and $d = 2$.

Harbus et al (1973) studied the four-dimensional phase diagram, in the $T\text{-}H\text{-}H_{st}\text{-}R$ space, and some thermodynamic properties of this model. In particular, they identified a tetracritical point, where two ferromagnetic and two antiferromagnetic phases become identical, at $R=H=H_{st}=0$ and T is equal to the critical temperature T_c of the two-dimensional Ising model. Using the symmetry properties of the model Hamiltonian (4.1), one can easily establish the following relation

$$\mathcal{Z}(T,R,H=H_o,H_{st}=0) = \mathcal{Z}(T,-R,H=0,H_{st}=H_o) \ , \qquad (4.2)$$

where $\mathcal{Z}$ is the canonical partition function. From Eq. (4.2) we may write

$$\chi(T,R,H=H_o,H_{st}=0) = \chi_{st}(T,-R,H=0,H_{st}=H_o) \ , \qquad (4.3)$$

where χ and χ_{st} are the direct and the staggered susceptibilities of the model system. Thus, in zero fields, Harbus and Stanley (1973) formulate the scaling hypotheses

$$\chi(\tau,R) \approx |\tau|^{-\gamma} \, Z\left(\frac{R}{|\tau|^{\phi}}\right) \qquad (4.4)$$

for $R>0$, and

$$\chi_{st}(\tau,R) \approx |\tau|^{-\gamma} \, Z\left(-\frac{R}{|\tau|^{\phi}}\right) \qquad (4.5)$$

for $R<0$, with $\tau \equiv (T-T_c)/T_c$, and $\gamma=\phi=1.75$. The critical

lines which are incident on the tetracritical point are associated with the singularity of the scaling function at z_t. They are described, therefore, in the vicinity of this multicritical point, by the symmetrical curves

$$\tau^{\phi} = \pm \frac{R}{z_t} \quad . \tag{4.6}$$

Although the one-variable series analyses, which were performed by Krasnow et al (1973), seem to support the scaling prediction, we decided to construct PDA's for the two-variable series expansions obtained by Harbus and Stanley (1973). Besides checking the previous analyses, the PDA's are expected to produce numerical results for the crossover exponent ϕ and the shapes of the phase boundaries near the tetracritical point.

We considered a triangular series of order 10 for the reduced susceptibility, $\bar{\chi} = \frac{kT\chi}{N}$, of the model system defined by the Hamiltonian (4.1) on an fcc lattice. Using the variables

$$x \equiv \tanh \frac{J}{kT} \qquad \text{and} \qquad y \equiv \tanh \frac{RJ}{kT} \tag{4.7}$$

we constructed 61 approximants of orders 7, 8 and 9. This is the complete set of PDA's, up to these orders, with $L \geq 1$ and $M = N \geq 3$. In Fig. 3 the estimates for the location of the tetracritical point are presented. The exactly known tetracritical point,

$$x_t = \sqrt{2} - 1 \quad , \quad y_t = 0 \quad ,$$

is also indicated in this figure, as well as intevals of $\pm 1\%$ and $\pm 10\%$ of x_t. We do not note any alignment of the estimates along the critical line, although they clearly tend to be situated on the half-plane $y > 0$ (which indicates the influence of the ferromagnetic critical line). In Fig. 4 we see estimates for γ as a function of estimates for x_t. The values $\gamma = 1.25$ and $\gamma = 1.75$ are indicated. The estimates for γ are plotted against the estimates for y_t in Fig. 5. In Fig. 6, estimates for ϕ are plotted against estimates for γ. The straight line $\gamma = \phi$ was drawn in order to test the agreement of the results with the scaling prediction $\gamma = \phi = 1.75$. Some correlations are observed in this figure, but they do not allow any conclusions. Finally, one may observe that the estimates for e_1 and e_2 vary in a rather large interval. However, all estimates are such that $|e_1| < 1$ and $|e_2| > 1$. In particular, those approximants whose estimates for the tetracritical point are close to the exact known location yield values for e_1 and e_2 such that $|e_1| \ll 1$ and $|e_2| \gg 1$. This seems to indicate that the original x and y axes are indeed the proper scaling axes.

We believe that the nature of the tetracritical point as a terminal point of the ferromagnetic line may be one of the reasons for the rather poor performance of the aproximants in this problem. In order to work with a quantity which takes into account the symmetry of the model, we defined the average reduced susceptibility,

$$\bar{\chi}_m = \frac{1}{2}\,(\bar{\chi} + \bar{\chi}_{st}) \qquad (4.8)$$

which diverges at the critical line for both $R > 0$ and $R < 0$. From (4.3), the series expansion for $\bar{\chi}_m$ may be obtained trivially from the series for $\bar{\chi}$ by a mere supression of all odd terms in y. Thus, from the defining equations of the PDA's it is possible to have P_L and Q_M even in y and R_N odd. This really happens numerically, and leads to the fixed value $y_t = 0$ in the estimates for the tetracritical point. In the approximants for $\bar{\chi}_m$ we noted a large number of cases where ill-conditioned equations were obtained. It was impossible to construct any approximant of order 8, but there were 55 approximants of order 9 which, despite being off-diagonal, displayed well conditioned linear equations. Fig. 7 shows estimates for γ as functions of estimates for x_t. The marked point $x_t = \sqrt{2} - 1$, $\gamma = 1.75$ indicates that the results are really consistent with the expected values. The apparent dispersion of the estimates and the linear correlation they reveal is known from d-log Padé results for one variable series. Fig. 8, where we plotted estimates of ϕ versus estimates of x_t, shows a similar behavior. Finally, Fig. 9, which displays estimates of γ versus estimates of ϕ, seems to indicate very strongly that we really have $\gamma = \phi = 1.75$ for this model. It is to be emphasized that in this case the values $e_1 = 0$ and $e_2 \to \infty$ are fixed by symmetry.

We also constructed flow diagrams for some of the best approximants to the original series for $\bar{\chi}$ and for

$\bar{\chi}_m$. It is remarkable that the best approximants exhibit locally stable tetracritical point estimates. The starting points of the flow-lines were located on a circle of radius $r = 0.32862$ and centered at $(\sqrt{2} - 1 , 0)$, which contains the estimated critical point ($x_c = 0.10174$, $y_c = 0.10174$) of the isotropic Ising model on an fcc lattice (Sykes (1972)).

Fig. 10 shows the flow-diagram for an approximant of order 9 ($L = 25$, $M = N = 15$) for the series expansion of $\bar{\chi}$. This approximant gives the estimates

$$x_t = 0.411873 \quad ,$$

$$y_t = -3.56741 \times 10^{-5}$$

and

$$e_1 = -1.415158 \times 10^{-2} \quad , \quad e_2 = 2.34177 \ ,$$

$$\gamma = 1.87897 \quad , \quad \phi = 1.79030 \ .$$

It is apparent the alignment of most flow-lines with the scaling axis with slope e_1 . The marked flow-line corresponds to the estimated critical boundary. A log-log plot of $x-x_t$ versus $y-y_t$ for this particular line provides another estimate for ϕ . The points are linearly correlated, even in regions not so close to the tetracritical point. If one estimates the slope grafically, it is possible to obtain $\phi = 1.6 \pm 0.2$.

Finally, Fig. 11 shows the flow-diagram for an

approximant of order 9 ($L = 21$, $M = 30$, $N = 5$) for the series expansion of $\overline{\chi}_m$. The estimated tetracritical parameters are

$$x_t = 0.4146114 \ ,$$
$$\gamma = 1.7659 \ ,$$
$$\phi = 1.7840 \ ,$$

while

$$y_t = 0 \ , \quad e_1 = 0 \ , \quad e_2 \to \infty \ ,$$

are fixed by the biased symmetry requirements. Due to the parity of the polynomials, the flow-diagram is symmetric, so only the half-plane $y > 0$ is displayed. The same features observed in the former flow-diagram are visible here, but a log-log plot of the estimated critical line produces the result $\phi = 1.75 \pm 0.02$, which manifests the better quality of these estimates.

V. SUMMARY

We used finite double-variable power series of some test functions and thermodynamic model functions to access the performance of the partial differential approximants for estimating multicritical parameters and phase boundaries.

The test functions were chosen so that their singular parts simulate the kind of multicritical behavior which is expected to occur in physical situations. Some test

functions could be represented exactly by PDA's. In this case we obtained excellent numerical results with approximants of lower orders. The accuracy of the estimates for the test functions which could not be represented exactly by approximants of finite order tended to improve as we increased the order of the approximants. This happened even in cases where approximants of relatively lower orders provided quite erratic estimates. Also, we used the method of characteristics to obtain numerical solutions for the defining differential equations of some approximants. It was possible to verify a strong correlation between the quality of the estimates for the multicritical parameters and the accuracy of these numerical solutions.

With the purpose of analyzing the crossover behavior between two and three dimensions, we constructed PDA's for the series expansion of the direct susceptibility of the axial anisotropic Ising model. The quality of the estimates improved considerably as we turned to the analysis of the more symmetric series expansion corresponding to the sum of the direct and the staggered susceptibilities. Besides using the PDA's for obtaining numerical estimates of the multicritical parameters, we also performed numerical solutions of the defining differential equations for some approximants. This procedure gives an estimate of the critical line in the anisotropy(R)-temperature(T) plane and an additional estimate of the crossover exponent ϕ. It is worth remarking that, despite the good overall agreement with the scaling predictions, the existent series expansions are a bit too short

for providing really excellent estimates by means of the PDA's.

ACKNOWLEDGMENTS

We whish to thank the financial support of FAPESP (Brazil).

REFERENCES

Baker G A Jr 1975 Essentials of Padé Approximants (New York: Academic)

Baker G A Jr and Hunter D L 1973 Phys.Rev. B7 3377-92

Brand L 1966 Differential and Difference Equations (New York: Wiley) p 201

Chisholm J S R 1973 Math.Comp. 27 841-8

Fisher M E 1977a Statistical Mechanics and Statistical Methods in Theory and Application ed U Laudman (New York: Plenum) p 3

Fisher M E 1977b Physica 86-88b 590-2

Fisher M E and Kerr R M 1977 Phys.Rev.Lett. 39 667-70

Harbus F, Hankey A, Stanley H E and Chang T S 1973 Phys.Rev. B8 2273-8

Harbus F and Stanley H E 1973 Phys.Rev. B7 365-70

Hunter D L and Baker G A Jr 1973 Phys.Rev. B7 3346-76

Krasnow R, Harbus F, Liu L L and Stanley H E 1973 Phys.Rev. B7 370-9

Roberts D E, Griffiths H P and Wood D W 1975 J.Phys.A: Math. Gen. 8 1365-72

Sykes M F, Gaunt D S, Roberts P D and Wyles J A 1972 J.Phys. A: Math.Gen. 5 640-52

TABLE CAPTIONS

TABLE I - Specifications of the approximants to the power series of the test functions. The approximants were numbered from 1 to 88; L, M and N stand for the number of terms in the polynomials P_L, Q_M and R_N, respectively.

TABLE II - Estimates for the "critical parameters" of the test function $F_e = (1 - x - \frac{1}{2} y)^{-3/2} (1 - 2x - \frac{1}{5} y)^{-1/2} + \exp(-x - 2y) \cos xy$, provided by a subset of the approximants defined in Table I.

TABLE III - Estimates for the "critical parameters" of the test function $F_f = (1 - x - 2y)^{-5/2} (1 - 3x - y)^{-2} + \exp(-x - 2y) \cos xy$, for the same subset of PDA's presented in Table II.

TABLE IV - Ordered sequences of PDA's to function F_e, according to the decreasing precision of their estimates. The parameters used in the ordering procedure are: Δ_c - distance between the estimated and the exact "multicritical point"; Δ_1 - distance between the estimated "multicritical point" and the straight line $1-x-\frac{1}{2} y=0$; Δ_2 - distance between the estimated "multicritcal point" and the straight line $1-2x-\frac{1}{5} y=0$; Δ_{exp} - distance between the estimated exponents (γ,ϕ) and the straight line $\gamma - \frac{1}{2}\phi = \frac{3}{2}$ for the scaling option with $e_1 \sim -10$ and $e_2 \sim -2$; Δe_1 - absolute difference between the exact and the estimated values for e_1;

Δe_2 - absolute difference between the exact and the estimated values for e_2 ; Δe - equals to $\sqrt{(\Delta e_1)^2 + (\Delta e_2)^2}$.

TABLE V - Ordered sequences of PDA's to function F_f , according to the decreasing precision of their estimates. The parameters used in the ordering procedure are the same as defined in the caption of Table IV, with the exception of: Δ_1 - distance between the estimated multicritical point and the straight line $1-x-2y=0$; Δ_2 - distance between the estimated multicritical point and the straight line $1-3x-y=0$; Δ_{exp} - distance between the estimated exponents (γ,ϕ) and the straight line $\gamma-2\phi=\frac{5}{2}$ for the scaling option with $e_1 \sim -3$ and $e_2 \sim -\frac{1}{2}$.

FIGURE CAPTIONS

FIG.1 - Flow diagram in the (x,y) plane of the PDA nº 1 (L=1 , M = N = 3) for the function F_c . The heavier lines indicate the trajectories which correspond to the scaling axes. The dots on the flow lines are spaced in unitary "time" intervals.

FIG.2 - Flow diagram in the (x,y) plane of the PDA nº 73 (L = 35 , M = 34 , N = 37) for the function F_d . The symbols have the same meaning as in Fig. 1.

FIG.3 - Estimates for the location of the tetracritical point (x_t, y_t) for the series expansion of the suscepbtibility of the axial anisotropic spin-1/2 Ising model on the fcc lattice. The crosses, open dots, and full dots indicate PDA's of orders 9,8, and 7 respectively. Intervals of ±10% and ±1% about the exact value of x_t are also indicated.

FIG.4 - Estimates for the tetracritical exponent γ plotted against estimates for x_t . The symbols are the same as in Fig.3. The dashed lines indicate the values of the critical exponent γ for the two and the three-dimensional Ising model, and the exact value of x_t for the two-dimensional Ising model.

FIG.5 - Estimates for the tetracritical exponent γ plotted against estimates for y_t . The symbols have been defined in the captions of Figs. 3 and 4.

FIG.6 - Estimates for the tetracritical exponent γ plotted against estimates of the crossover exponent ϕ. The scaling prediction $\gamma = \phi = 1.75$ is also indicated in this figure.

FIG.7 - Estimates for the tetracritical exponent γ plotted against estimates for x_t. All crosses represent results from approximants of order 9 to the series expansion of the average susceptibility $\left(\frac{1}{2}\chi + \frac{1}{2}\chi_{st}\right)$ of the axial anisotropic Ising model on the fcc lattice. The big cross indicates the exact location of x_t and the scaling prediction for γ.

FIG.8 - Estimates for the crossover exponent ϕ plotted against estimates of the tetracritical parameter x_t. The order of the approximants as well as the series expansion which has been used and all the symbols of this figure are the same as in Fig.7.

FIG.9 - Estimates for the crossover exponent ϕ plotted against estimates for the tetracritical exponent γ. We are using approximants of order 9 for the series expansion of the average susceptibility of the axial anisotropic Ising model. The scaling prediction $\gamma = \phi = 1.75$ is indicated by the big cross.

FIG.10 - Flow diagram, in the ($x = \tanh J/kT$, $y = \tanh RJ/kT$) plane associated with a PDA of order 9, given by $L = 26$, $M = N = 15$, for the series expansion of the reduced direct susceptibility of the axial anisotropic

Ising model on the fcc lattice. The dot-dashed lines indicate the estimated scaling axes. The heavy line indicates the estimated phase boundary.

FIG.11 - Flow diagram, in the ($x = \tanh J/kT$, $y = \tanh RJ/kT$) plane, associated with a PDA of order 9, given by $L = 21$, $M = 30$, $N = 5$, for the series expansion of the reduced average suceptibility of the axial anisotropic Ising model on the fcc lattice. The scaling axes are fixed by symmetry. The heavy line indicates the estimated phase boundary.

I	L	M	N	I	L	M	N	I	L	M	N	I	L	M	N
1	1	3	3	23	23	22	22	45	3	26	50	67	15	74	3
2	4	6	6	24	22	23	22	46	59	10	10	68	36	35	35
3	2	5	15	25	22	22	23	47	10	59	10	69	35	36	35
4	2	10	10	26	25	21	21	48	10	10	59	70	35	35	36
5	7	5	25	27	21	25	21	49	66	7	6	71	37	34	35
6	7	15	15	28	21	21	25	50	30	31	31	72	34	35	37
7	7	25	5	29	37	15	15	51	31	30	31	73	35	34	37
8	4	21	21	30	49	15	3	52	31	31	30	74	35	37	34
9	6	5	35	31	15	3	49	53	29	31	32	75	34	36	36
10	6	20	20	32	3	49	15	54	31	29	32	76	36	34	36
11	6	35	5	33	3	32	32	55	32	29	31	77	36	36	34
12	16	15	15	34	15	26	26	56	32	31	29	78	45	31	30
13	36	5	5	35	27	26	26	57	29	32	31	79	45	30	31
14	6	5	45	36	26	27	26	58	31	32	29	80	28	39	39
15	6	15	35	37	26	26	27	59	28	32	32	81	30	30	38
16	6	25	25	38	23	28	28	60	20	36	36	82	38	34	34
17	6	35	15	39	37	21	21	61	36	28	28	83	50	28	28
18	6	45	5	40	21	37	21	62	10	41	41	84	3	52	51
19	14	21	21	41	21	21	37	63	45	23	24	85	3	51	52
20	18	4	34	42	3	38	38	64	45	24	23	86	10	21	75
21	18	19	19	43	67	6	6	65	3	15	74	87	21	75	10
22	18	34	4	44	3	50	26	66	74	3	15	88	21	10	75

TABLE I

I	x_c	y_c	e_1	e_2	γ	ϕ
12	0.3186	2.318	10.66	-2.128	5.537	-7.091
15	0.4612	0.6485	-2.566	-5.6×10^{-2}	0.5964	0.5928
23	0.4668	0.4075	-19.80	-0.7800	3.139	5.695
27	0.1893	-4×10^{-4}	30.39	1.004	0.1857	2.164
30	0.5921	-0.9837	-10.08	-0.5056	-0.7342	-2.605
34	0.4547	0.3446	-6.248	0.9314	-0.3029	-0.9209
37	0.3913	1.413	-22.18	-2.002	-0.5770	-5.599
49	0.8315	-1.419	-1.286	1.082	-1.025	-2.038
50	0.3406	1.305	-5.917	-2.004	1.185	-0.5753
66	0.4570	0.7495	-18.78	-3.845	0.3050	-0.6100
68	0.3806	1.265	-12.08	-1.998	0.2370	-2.653
72	0.3735	1.256	-9.685	-1.995	-0.3188	-3.646
76	0.4268	1.244	17.86	-1.748	0.9843	-2.899
82	0.3739	1.248	-9.557	-1.995	4.5×10^{-2}	-2.786
85	0.3742	1.224	-9.224	-2.026	-0.261	-3.229
87	0.4061	1.036	-16.14	-2.149	-0.3537	-2.350

TABLE II

I	x_c	y_c	e_1	e_2	γ	ϕ
12	0.1884	0.4059	-2.950	-0.5044	0.4094	-1.104
15	0.2035	0.4457	-3.712	-0.4022	-1.273	-2.043
23	0.1989	0.3987	-2.966	-0.5030	-0.5720	-1.547
27	0.2000	0.4000	-3.001	-0.5003	-0.2923	-1.398
30	0.2353	0.3693	-4.141	-0.5071	0.9854	-0.3429
34	0.2000	0.3999	-3.001	-0.5003	-6.67×10^{-2}	-1.217
37	0.2001	0.3999	-3.004	-0.5004	6.53×10^{-2}	-1.216
49	9.34×10^{-2}	0.6537	-2.662	-0.2878	-79.82	-1.525
50	0.2001	0.4001	-3.007	-0.4991	1.017	-0.7439
66	0.2635	0.3179	-4.307	-0.5884	-3.484	-0.9281
68	0.2000	0.4006	-3.020	-0.5000	-13.81	-8.160
72	0.2001	0.4004	-3.018	-0.4999	-11.03	-6.767
76	0.2001	0.4000	-3.002	-0.5000	-0.8118	-1.655
82	0.2021	0.3974	-1.467	7.85×10^{-2}	4.583	1.066
85	0.2003	0.4008	-3.018	-0.4959	-0.1895	-1.344
87	0.2341	0.3296	-10.89	-5.04×10^{-2}	4.621	1.526

TABLE III

ORDERED APPROXIMANTS ACCORDING TO INCREASING VALUES OF Δ_c

82	72	73	75	74	77	69	53	68	70	55	57	81	86	85	71	64	79	41
78	76	83	50	52	62	58	88	84	60	38	37	28	87	54	80	63	14	29
24	31	45	9	59	61	47	66	15	13	25	23	20	26	34	2	21	6	12
17	39	27	5	43	44	42	48	16	22	35	40	19	4	46	3	8	33	36
32	11	10	30	1	49	65	67	56	51	7	18							

INCREASING VALUES OF Δ_1

72	82	57	88	50	75	74	73	77	86	69	81	70	68	85	55	53	41	71
64	79	83	52	62	78	58	20	60	76	16	84	14	87	31	47	18	37	54
40	80	38	28	24	29	22	63	66	59	61	45	15	36	2	13	67	25	17
23	21	26	34	6	9	39	12	42	48	35	3	4	19	46	33	27	8	11
49	32	30	10	5	43	44	65	56	51	1	7							

INCREASING VALUES OF Δ_2

13	57	72	41	39	4	82	42	11	46	35	19	85	75	74	83	73	77	69
81	58	30	64	79	70	68	54	52	71	23	55	62	24	87	34	33	80	26
21	29	53	78	6	60	48	61	86	25	59	84	15	50	10	66	37	14	31
88	28	3	63	12	32	76	65	38	45	56	2	17	49	51	47	7	20	27
9	22	5	43	44	40	16	67	36	1	8	18							

INCREASING VALUES OF Δ_{exp}

72	58	20	50	86	52	74	65	70	82	68	73	69	77	57	75	81	53	71
85	55	45	79	31	28	83	41	60	47	62	78	14	84	54	87	37	46	66
30	80	38	33	24	8	48	59	29	15	23	61	32	34	9	42	6	19	26
39	22	4	1	5	16	17	25	43	44	88	49	63	3	35	27	11	76	36
13	40	56	2	12	51	10	21	7	67	18	64							

INCREASING VALUES OF Δe_1

30	12	76	46	72	33	39	19	41	42	82	24	57	51	85	13	35	54	56
21	73	64	74	75	81	4	86	52	77	71	55	69	79	70	7	53	68	48
10	60	58	29	80	27	6	11	26	34	84	78	61	83	50	32	28	62	59
38	63	8	87	2	40	15	18	47	36	49	66	22	67	65	23	1	5	16
17	25	43	44	88	37	14	3	31	45	20	9							

INCREASING VALUES OF Δe_2

64	70	68	37	50	72	82	62	73	74	69	55	77	60	53	81	71	85	75
79	83	57	52	86	41	24	78	28	87	84	58	80	38	29	31	20	54	48
35	65	32	45	8	6	42	39	61	33	23	13	47	46	30	2	4	19	3
66	40	15	59	26	67	18	1	5	16	17	25	43	44	88	22	9	34	49
36	11	63	14	56	51	12	76	10	27	7	21							

INCREASING VALUES OF Δ_e

72	41	82	24	57	85	54	35	42	39	73	64	33	74	75	81	30	46	13
86	52	19	77	71	55	69	79	70	53	68	4	48	60	58	29	80	6	84
78	83	50	61	26	28	62	32	34	59	11	38	8	87	2	40	15	47	18
63	66	65	36	67	49	22	23	1	5	16	17	25	43	44	88	37	56	51
12	3	76	14	10	27	31	45	7	21	20	9							

TABLE IV

ORDERED APPROXIMANTS ACCORDING TO INCREASING VALUES OF Δ_c

27	34	76	58	53	36	52	56	59	50	51	62	37	80	57	61	35	60	38
72	71	78	69	83	26	64	70	75	68	77	33	21	85	55	86	28	39	84
42	54	74	29	23	24	41	19	81	46	82	79	73	25	45	40	48	12	10
44	88	8	31	47	15	30	65	13	87	6	66	20	43	14	9	4	32	5
7	49	3	17	63	22	18	2	67	16	11	1							

INCREASING VALUES OF Δ_1

76	39	27	83	58	34	62	35	37	52	12	56	36	38	53	51	50	59	80
33	61	57	78	60	64	72	71	69	77	70	26	68	75	28	21	55	86	85
54	84	74	42	82	29	24	23	41	19	81	46	79	73	25	31	47	45	40
48	30	32	14	10	88	8	44	15	13	66	87	65	43	20	6	9	2	4
7	5	49	22	18	3	17	63	67	11	16	1							

INCREASING VALUES OF Δ_2

54	34	56	27	36	77	52	76	58	53	67	37	62	64	59	80	38	50	35
51	60	57	72	69	70	68	61	55	75	74	86	83	71	22	73	78	42	26
85	18	79	33	21	39	28	29	84	82	23	81	24	19	41	46	25	45	40
8	10	20	88	12	87	48	31	15	43	49	47	44	30	65	66	7	4	6
13	14	32	5	9	16	3	17	63	2	11	1							

INCREASING VALUES OF Δ_{exp}

52	53	51	69	60	56	77	58	62	85	76	80	36	37	27	59	61	57	72
50	38	83	26	21	78	84	64	70	71	86	19	68	29	24	23	28	74	75
39	42	55	82	45	44	46	33	10	41	88	79	12	34	8	54	81	73	48
40	25	7	15	47	35	31	6	14	30	4	87	5	20	32	16	65	9	3
17	18	63	67	22	66	1	43	2	11	49	13							

INCREASING VALUES OF Δe_1

34	27	36	76	56	53	58	52	37	33	77	62	60	59	35	38	22	51	55
67	50	61	57	80	86	64	83	78	26	69	85	72	74	70	73	68	75	24
42	71	29	23	39	21	84	40	12	81	46	28	19	79	25	41	32	2	8
10	1	45	14	20	49	43	65	44	88	48	16	47	15	7	4	31	30	6
66	82	11	3	17	18	63	13	5	54	87	9							

INCREASING VALUES OF Δe_2

75	76	68	74	72	70	55	69	58	27	34	77	36	51	37	83	35	80	62
52	56	39	53	50	38	59	24	61	57	78	60	26	21	41	23	42	71	85
86	12	84	30	28	33	81	29	19	73	46	45	47	79	25	31	64	43	48
10	40	8	66	15	13	88	44	4	49	20	6	65	87	11	3	17	18	63
16	54	82	9	7	22	5	67	1	32	2	14							

INCREASING VALUES OF Δ_e

34	27	36	76	56	53	58	52	37	77	62	60	59	35	38	51	55	50	61
57	33	80	86	83	78	26	69	72	74	85	70	68	73	75	24	42	71	29
23	39	21	84	64	12	81	46	28	19	79	40	25	41	10	8	45	43	49
20	44	88	48	65	47	15	16	4	22	31	7	67	30	6	66	82	11	1
3	17	18	63	32	13	2	5	14	54	87	9							

TABLE V

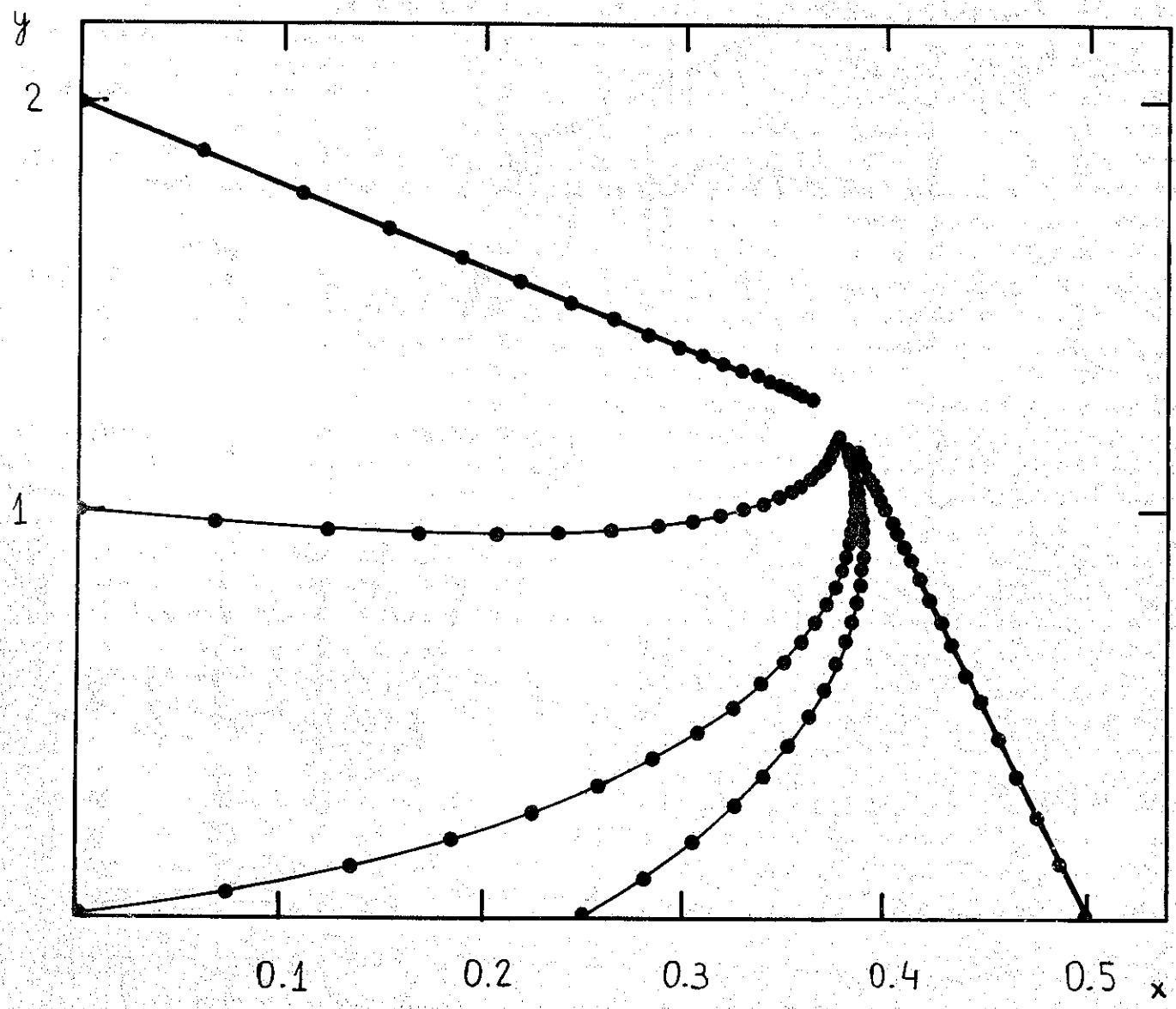

FIGURE 1

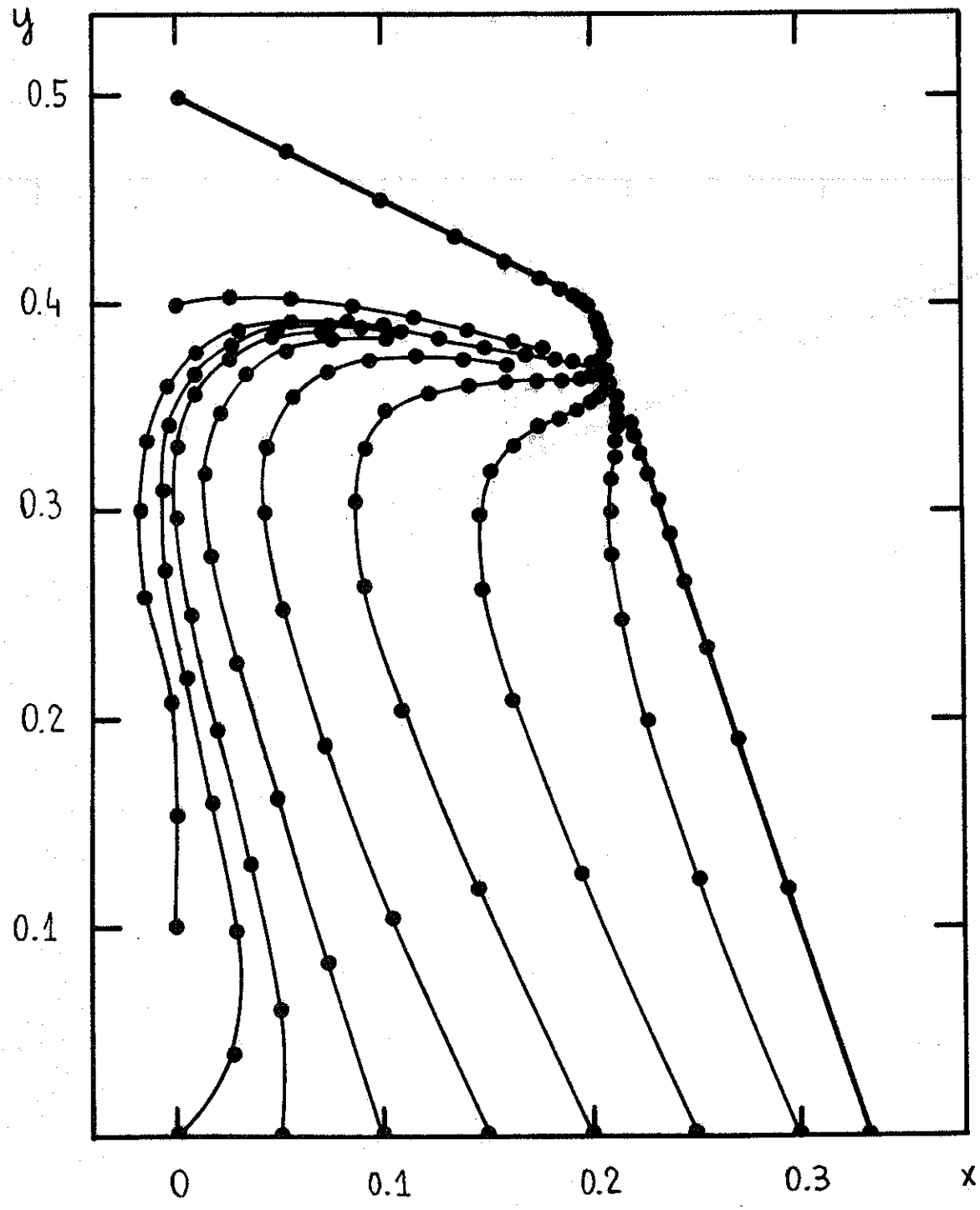

FIGURE 2

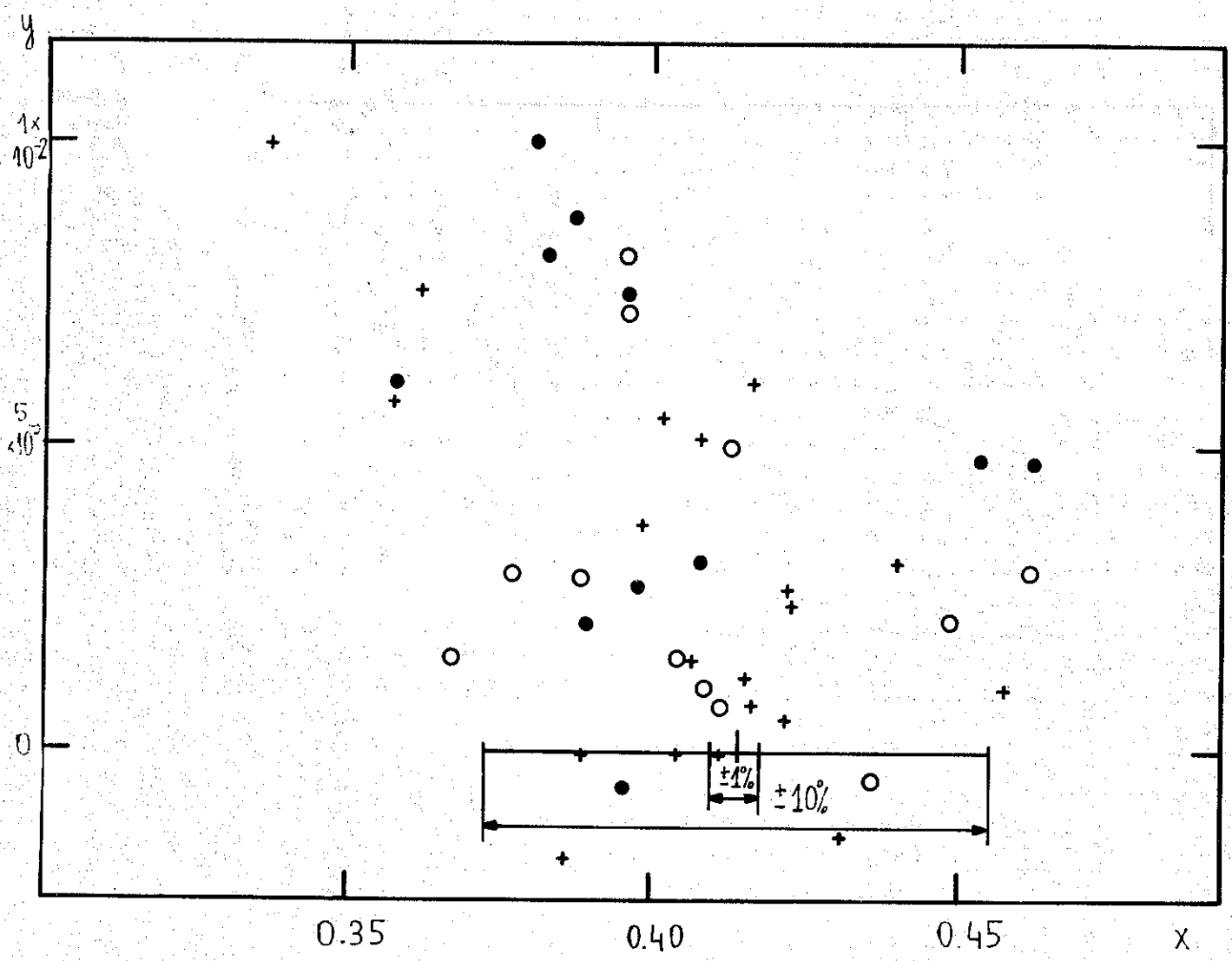

FIGURE 3

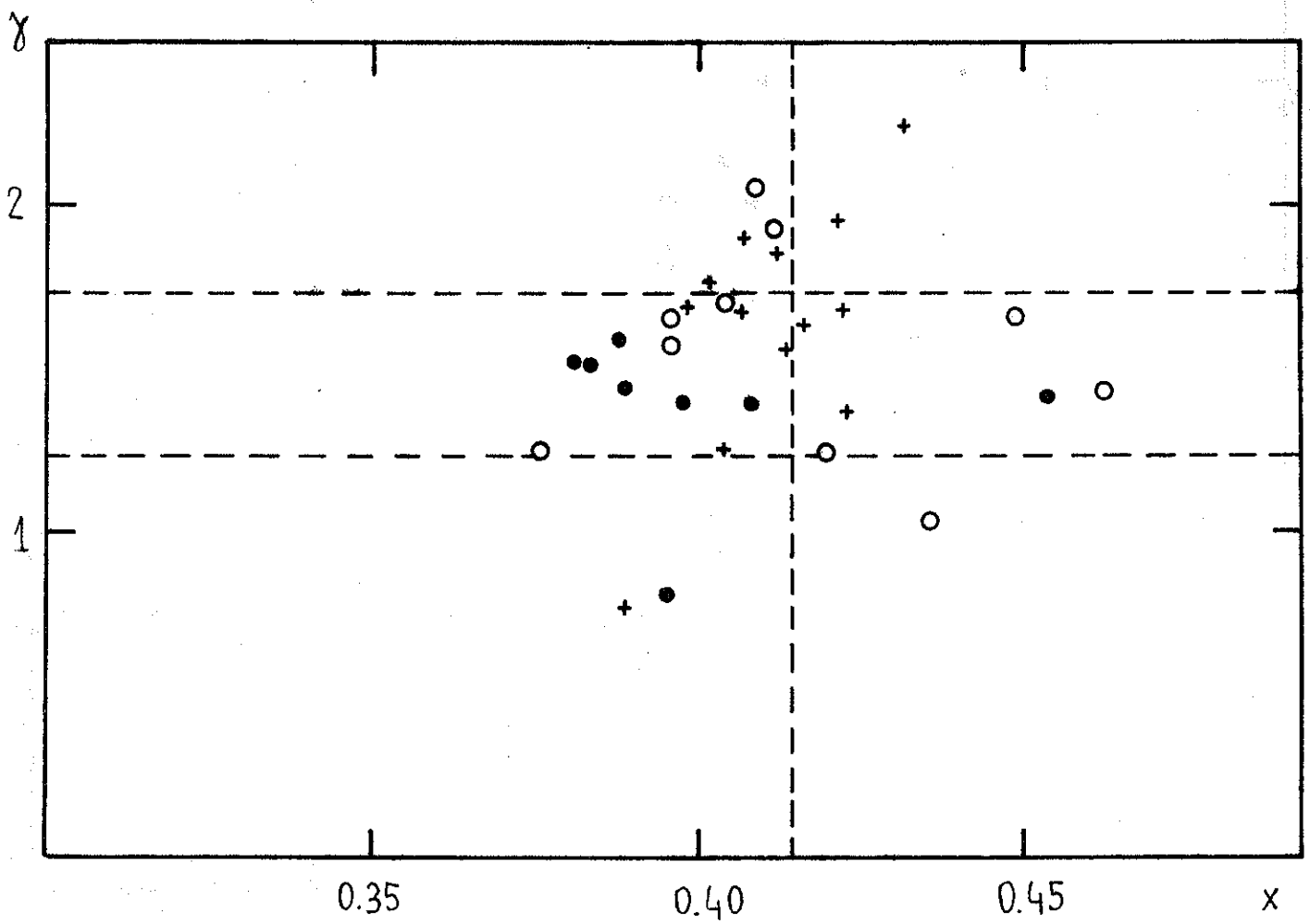

FIGURE 4

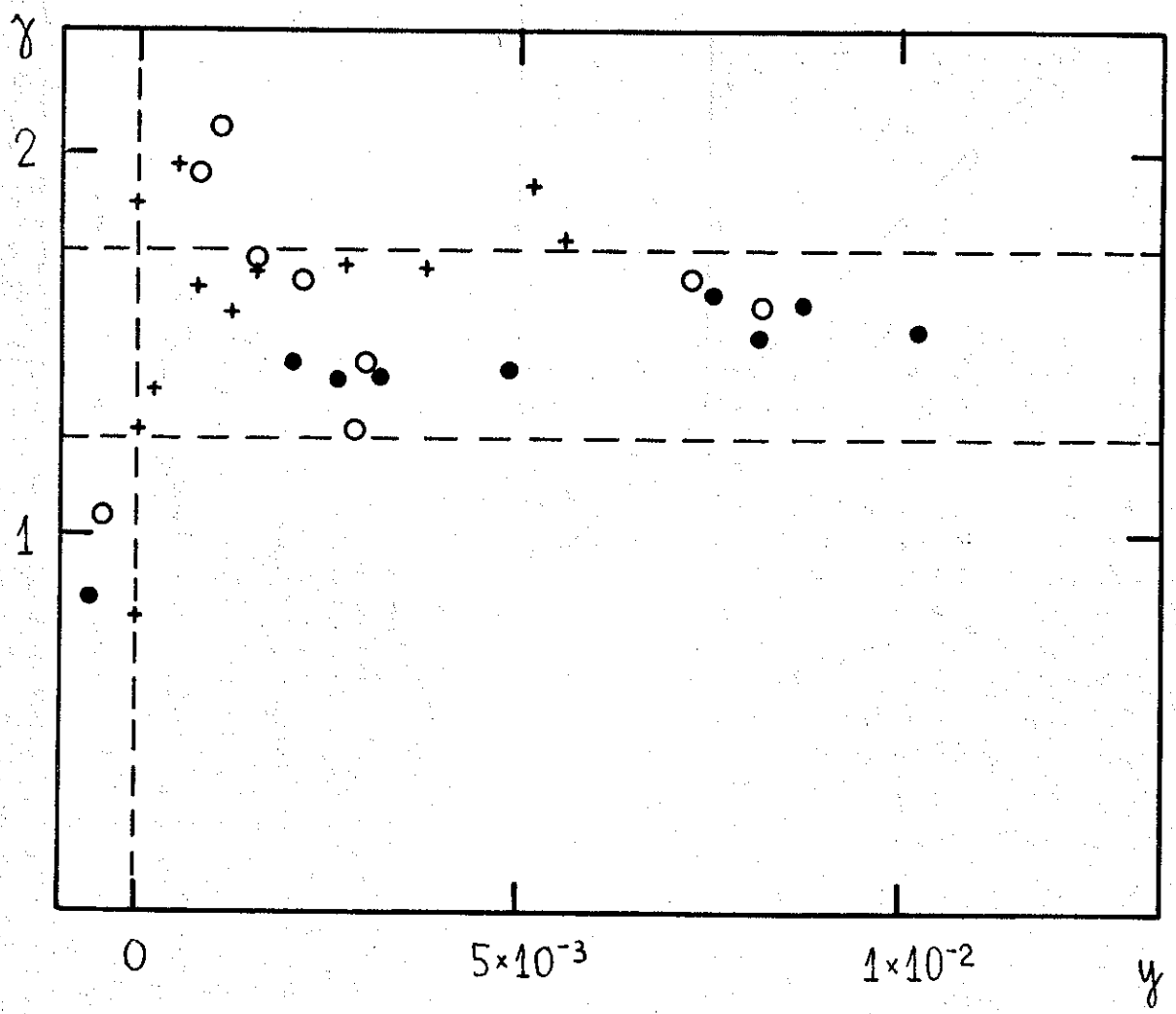

FIGURE 5

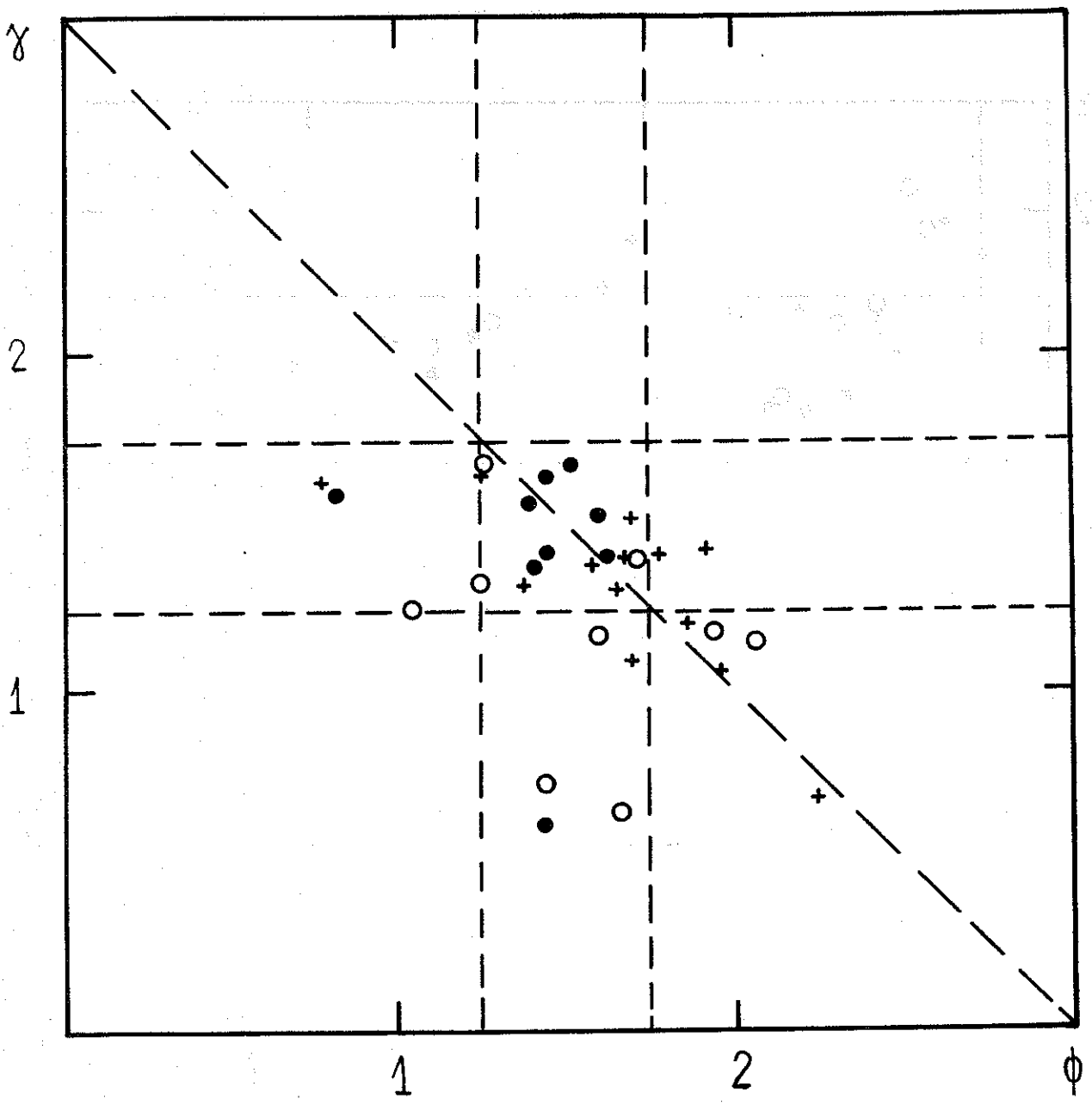

FIGURE 6

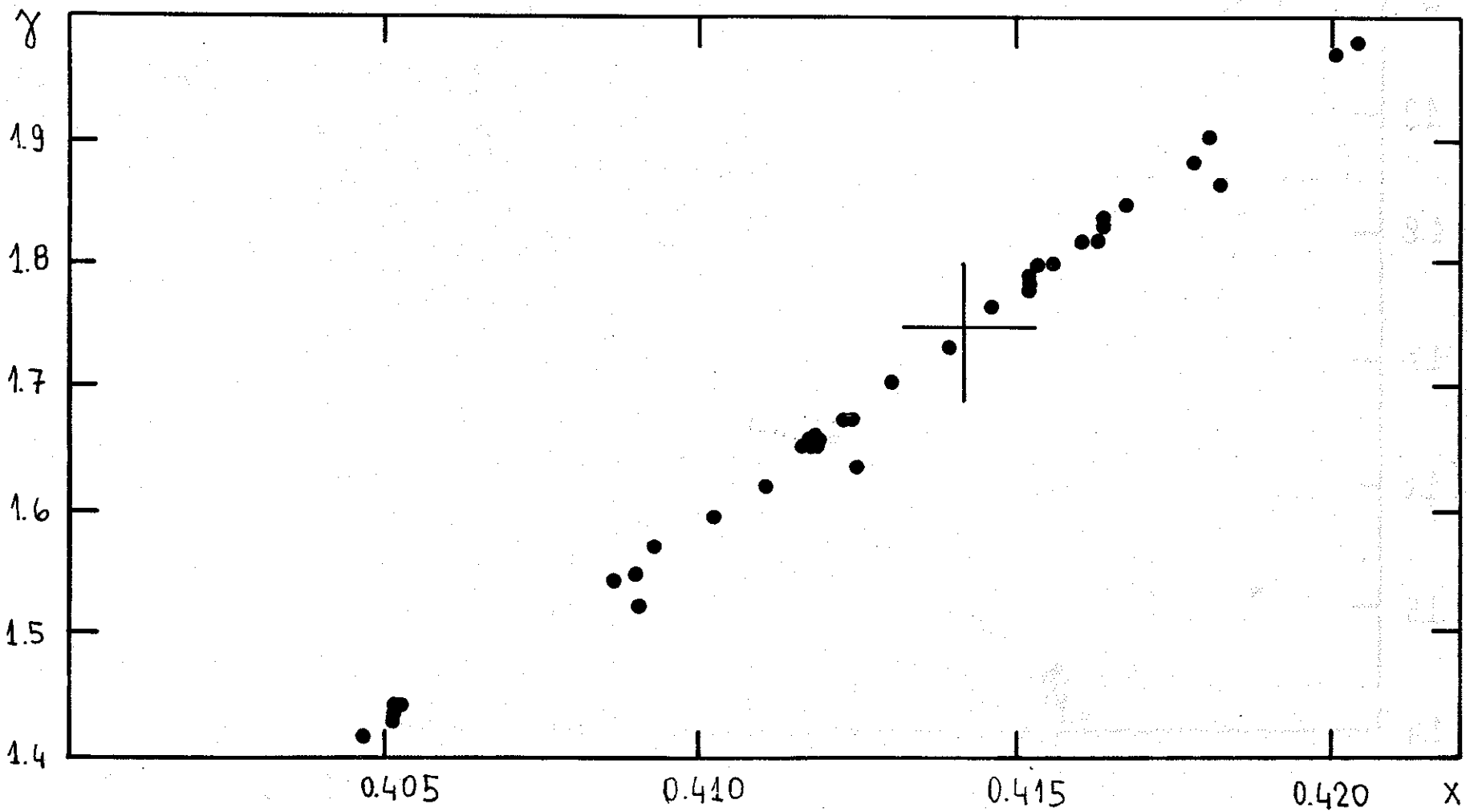

FIGURE 7

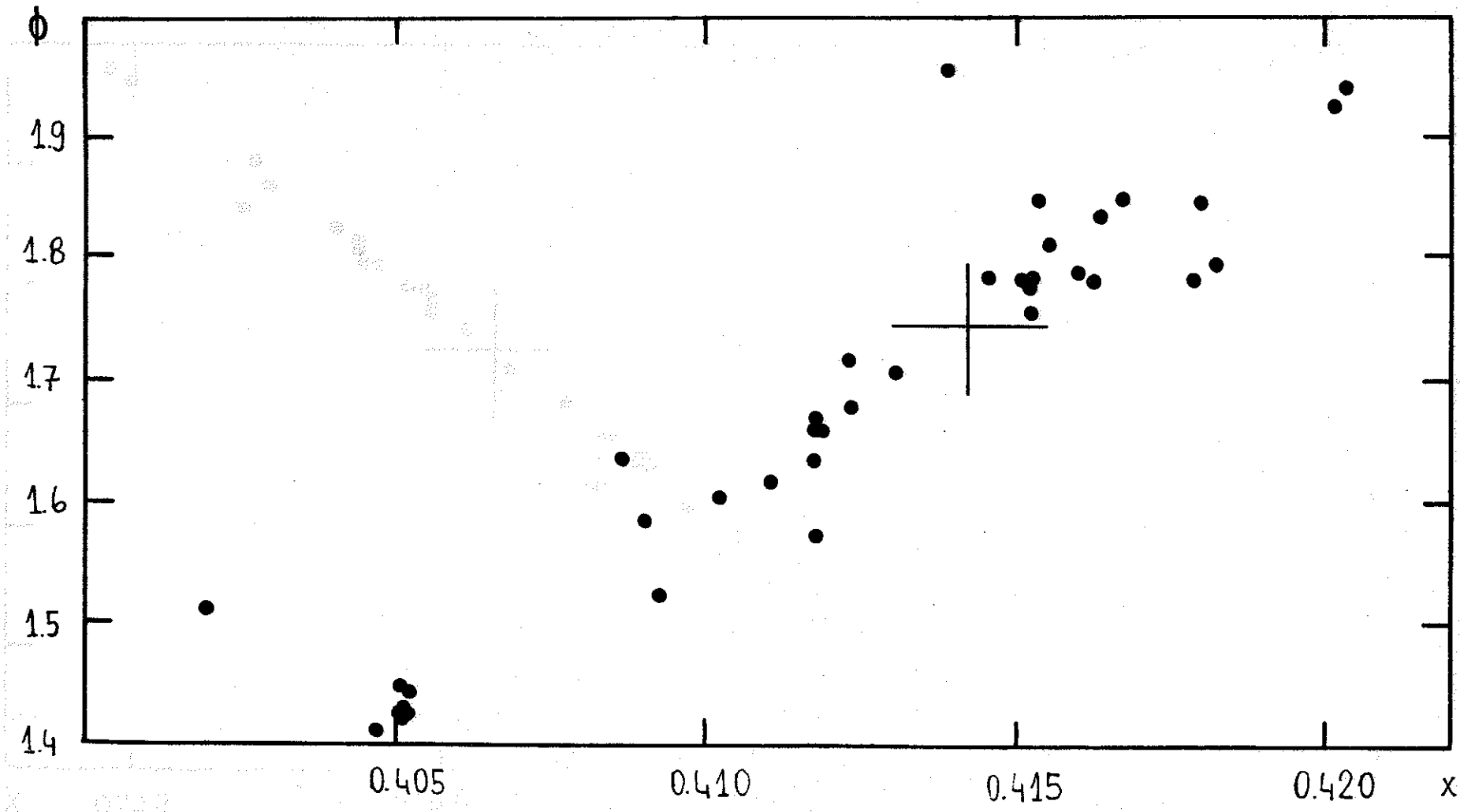

FIGURE 8

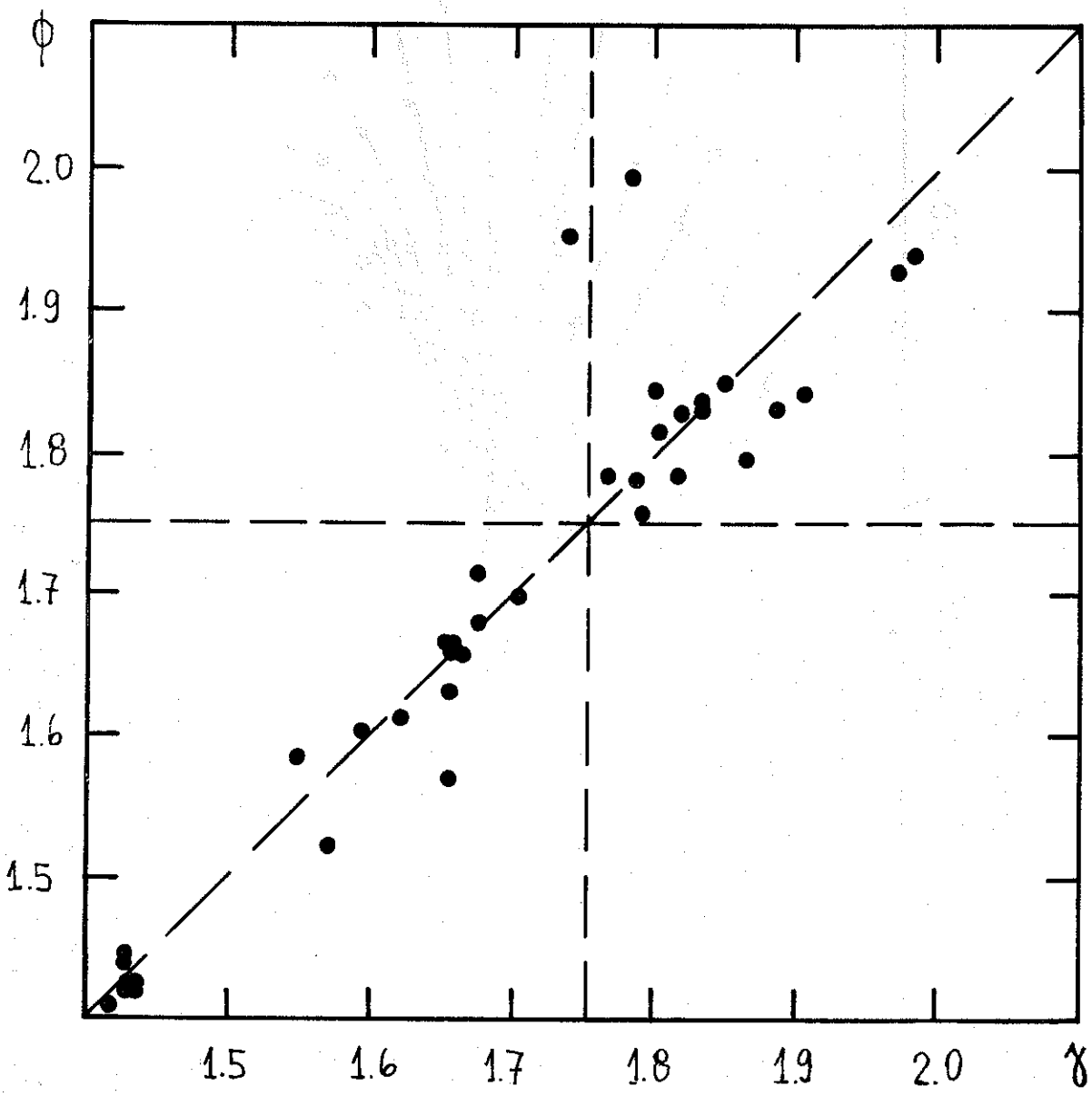

FIGURE 9

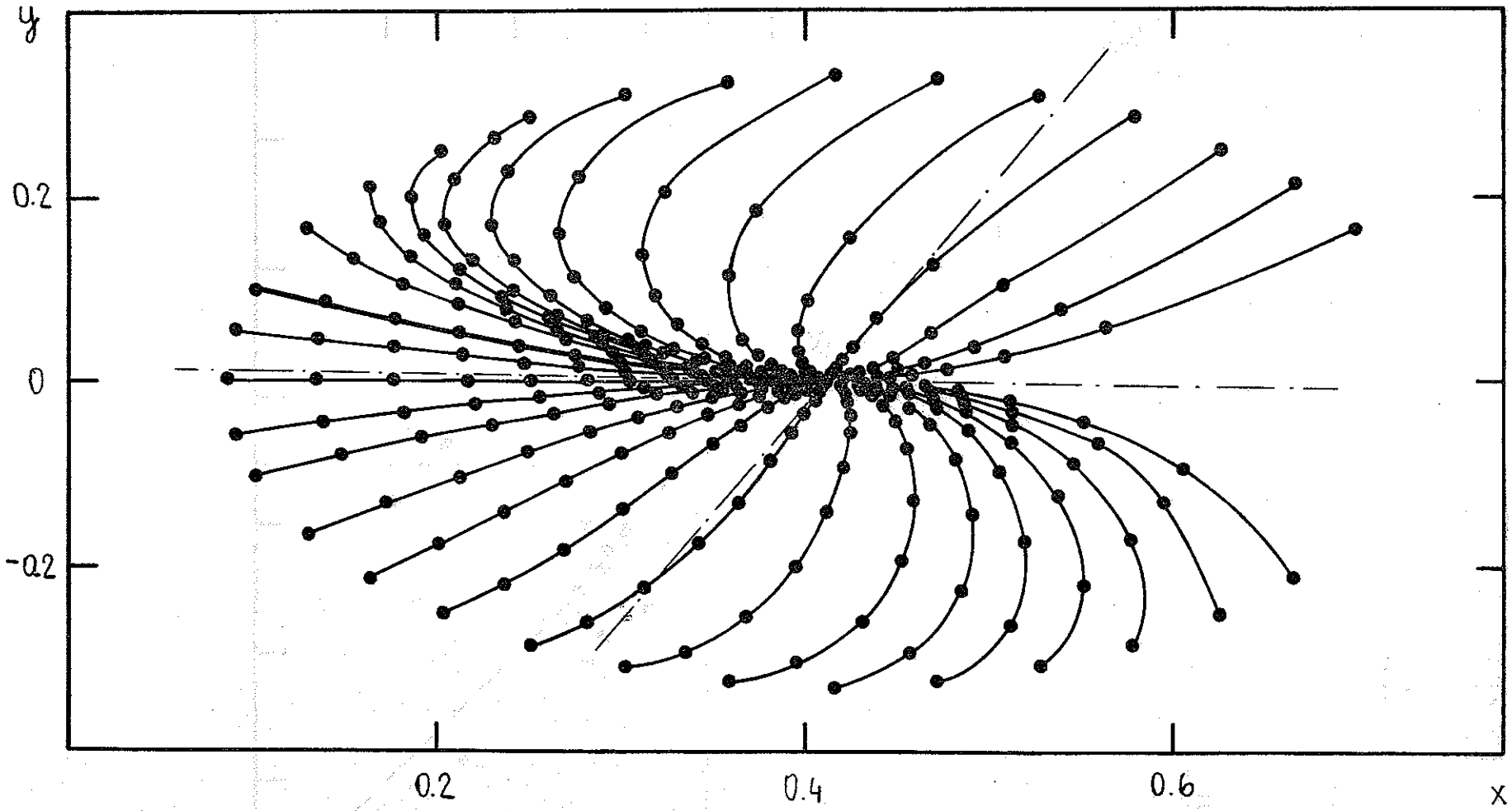

FIGURE 10

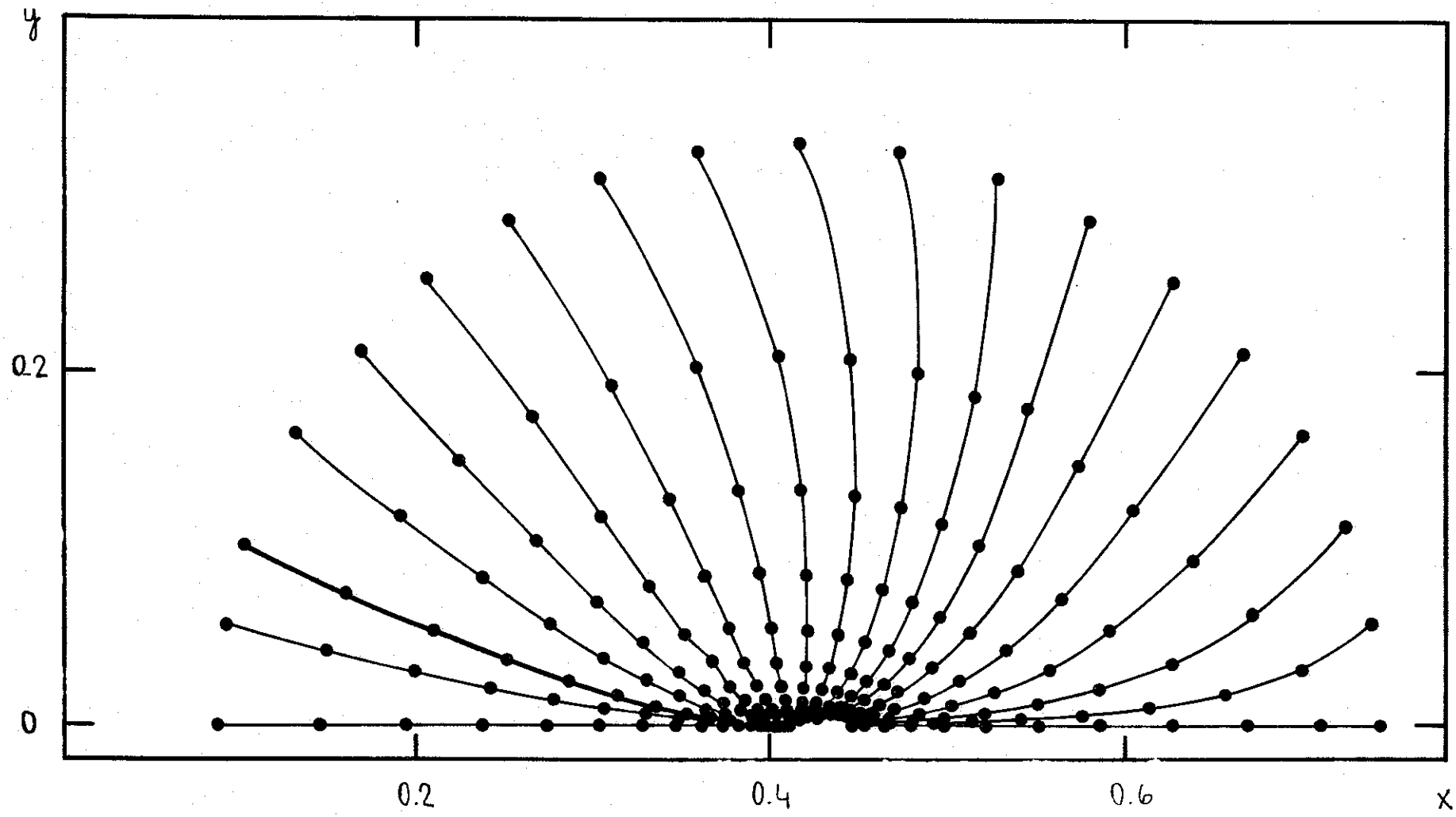

FIGURE 11